Received: 3 September 2019 | Revised: 30 December 2019 | Accepted: 2 January 2020

DOI: 10.1002/asl.953

Atmospheric Science Letters RMetS

RESEARCH ARTICLE

Dependence of sudden stratospheric warming type-transition on preceding North Atlantic Oscillation conditions

Hyesun Choi[1,2] | **Wookap Choi**[1] | **Seong-Joong Kim**[2] | **Baek-Min Kim**[3]

[1]School of Earth and Environmental Sciences, Seoul National University, Seoul, Republic of Korea

[2]Division of Polar Climate Sciences, Korea Polar Research Institute, Incheon, Republic of Korea

[3]Department of Environmental Atmospheric Sciences, Pukyong National University, Pusan, Republic of Korea

Correspondence
Baek-Min Kim, Department of Environmental Atmospheric Sciences, Pukyong National University, Pusan, Republic of Korea.
Email: baekmin@pknu.ac.kr

Funding information
Korea Polar Research Institute, Grant/Award Numbers: PE20090, PE20070; Comment: National Research Foundation of Korea, Grant/Award Numbers: 2018R1A2B6003197, 2019R1A2C1005460

Abstract

Most sudden stratospheric warming (SSW) events initiate with their centers being displaced from the pole. Some retain their displaced form until termination but some split into two vortices during their course. Here, we show that existence of a transition during the course of the SSW life cycle can be attributable to the condition of North Atlantic Oscillation (NAO) preceding before onset: Positive NAO favors SSW of displacement type with no transition while negative NAO favors the displacement–split type. We show that, in positive NAO precondition, vertical flux of wave activity immediately before onset is mostly contributed only by wavenumber 1 component, which contrasts with the relatively stronger contribution of wavenumber 2 in negative NAO precondition. Whole Atmosphere Community Climate Model (WACCM) simulation results are also consistent with the observational findings. Therefore, NAO can be regarded as a useful precursor for determining the type of forthcoming SSW events.

KEYWORDS

North Atlantic oscillation, precursor, sudden stratospheric warming, tropospheric-stratospheric dynamical processes, type-transition

1 | INTRODUCTION

Sudden stratospheric warming (SSW) is characterized by a rapid rise in polar stratospheric temperature and weakening of the circumpolar westerly wind during the boreal winter season (Matsuno, 1971). According to the classification devised by Choi *et al.* (2019), hereafter referred to as C19, SSW events can be categorized according to vortex behavior: vortex displacement is classified as displacement–displacement (DD) type, while vortex split is classified as either displacement–split (DS) or split–split (SS) type. They showed that this devised classification is appropriate for understanding SSW events because the three types differ distinctively during the prewarming period.

Because the definition and classification criteria of SSW types are described in detail in C19, we only briefly address them here. Major SSWs are defined when the zonal-mean zonal wind reverses from westerly to easterly at 10 hPa and 60°N during the boreal winter season (October–March). We define the first day of wind reversal as the central day (Day 0) of the SSW. The weakening of zonal flow during the course of the SSW life cycle is accompanied by deformation to the shape of the polar

vortex. C19 examined the temporal evolution of the polar vortex before (days −10 to −1) and after (days 0 to +10) the occurrence of SSWs and classified the events into three types based on the number of dominant planetary waves. The amplitudes of zonal wavenumbers 1 and 2 of geopotential height (GPH) averaged over 55°N–65°N at 10 hPa are used as the criteria for classification. In the type naming convention, the first and second letters indicate the shape of the polar vortex for waves 1 and 2, respectively, before and after the central day in the stratosphere. For example, for the DS type, D indicates vortex displacement for wave 1, while S indicates vortex split for wave 2 (C19).

Although there have been many studies on the classification of SSW types, including C19, the factors involved in determining the vortex breaking type remain unknown, especially for DS type. SS type, which is characterized by the presence of two separate vortices before the central day, is distinguishable from DD and DS types and is not related to the North Atlantic Oscillation (NAO) phases before the onset. In this study, therefore, we aim to investigate the troposphere precursors by focusing on the North Atlantic for DS-type and DD-type SSWs as will be discussed later.

Since SSWs are known to be related to variability in tropospheric circulation and weather (Baldwin and Dunkerton, 1999, 2001; Thompson *et al.*, 2002), predicting the occurrence of SSWs is an important issue in subseasonal to seasonal forecasting (Karpechko *et al.*, 2018; Taguchi, 2018; Rao *et al.*, 2019b). The ability to forecast stratosphere-troposphere coupling after warming events could be improved by understanding what mechanisms influence the change in the stratospheric polar vortex in advance. Thus, many studies have been performed toward understanding the differences in various SSW precursory patterns related to weakening and breaking of polar vortexes. These studies, however, have analyzed SSWs based on two traditional types, "vortex displacement type" and "vortex split type" (Charlton and Polvani, 2007), or involved a case study (Naujokat *et al.*, 2002; Martius *et al.*, 2009; Cohen and Jones, 2011; Attard *et al.*, 2016). In contrast, we apply the three-type C19 classification to investigate precursors.

Baldwin *et al.* (1994) showed that the zonal-mean stratospheric polar vortex is positively correlated with the NAO. Ambaum and Hoskins (2002) also showed that the stratospheric jet is strengthened by an increase in the NAO owing to the increased equatorward refraction of upward-propagating Rossby waves. However, how the NAO conditions relate to the subsequent development of different SSW types has not yet been reported in the literature. Therefore, we aim to investigate the role of the NAO in determining SSW type after the onset.

The predictability of SSW varies with event types (Taguchi, 2018; Domeisen *et al.*, 2019) and dominant wave numbers (Rao *et al.*, 2019a). C19 identified that significantly positive sea level pressure anomaly over the northeast pacific region occurred after the DS-type SSW events whereas the insignificant minor anomaly over that region appeared after DD-type SSW events (Figure 10 in C19). This suggests the possibility that DD and DS-type SSW events have different effects on tropospheric weather in terms of local scale. Therefore, the North Atlantic anomaly responsible for the type transition can provide useful information for prediction of SSW events and tropospheric weather on subseasonal to seasonal time scale.

The remainder of this paper is organized follows. Section 2 describes the data and model employed in the study. Section 3 discusses how the NAO appears to act as a precursor for the DD and DS types, and a summary and discussion are provided in section 4.

2 | DATA AND MODEL

We used two reanalysis datasets from the National Centers for Environmental Prediction-National Center for Atmospheric Research (NCEP-NCAR) from January 1, 1957 to December 31, 2014 (Kalnay *et al.*, 1996), as well as Modern-Era Retrospective analysis for Research and Applications (MERRA) assimilated data (inst3_3d_asm_Cp) from January 1, 1979 to December 31, 2014 (Rienecker *et al.*, 2011). The atmospheric variables and their spatial resolution are the same as those used in C19. The daily climatological values of each variable calculated based on periods of 1981–2010 for NCEP-NCAR and 1979–2011 for MERRA are smoothed by a 31-day running mean. In this study, all anomaly fields are defined by departure from these climatological means. The results in this paper are insensitive to the dataset. To show changes in variables in the vertical direction, we display the results from MERRA, which have a higher vertical top than the other reanalysis dataset.

In order to reconfirm features found in the reanalysis datasets, which cover rather short periods, we employed the Whole Atmosphere Community Climate Model (WACCM) for simulation (Neale *et al.*, 2010). The model design and spatial resolution of the output are identical to those of C19. The model was run for 361 years, and 350 boreal winters from the last 351 years were analyzed. In this study, we performed a Student's two-sided *t* test to determine statistical significance.

To characterize the strength and phase of the NAO, two daily NAO indices were downloaded from two websites. One from the NCEP/Climate Prediction Center

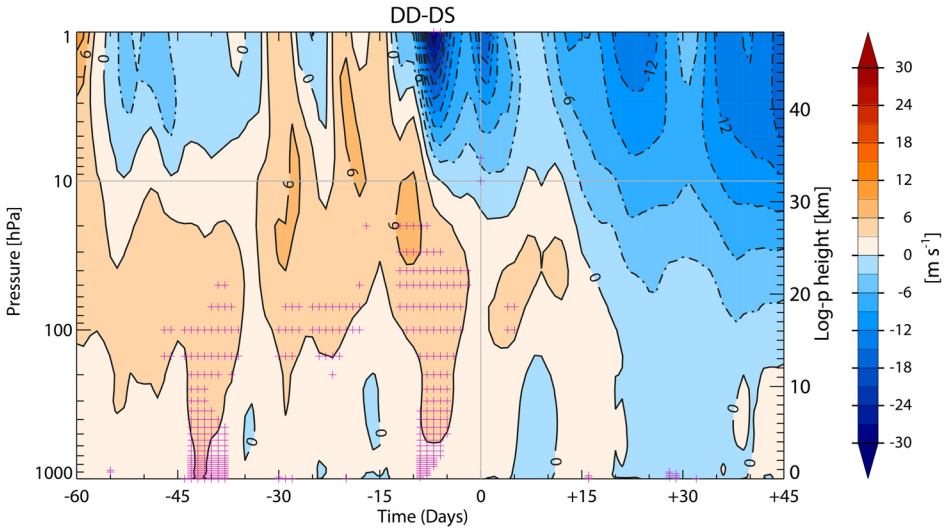

FIGURE 1 Composite differences of zonal-mean zonal wind averaged over 50°N–70°N between DD and DS events from MERRA (DD minus DS). Gray horizontal and vertical lines denote the 10 hPa level and central day, respectively. The contour interval is 3 m s^{-1}. Pink crosses indicate statistically significant regions at 95% confidence level. Dashed-dotted contours denote negative values

(CPC) (https://www.cpc.ncep.noaa.gov/products/precip/CWlink/pna/nao.shtml) was constructed by projecting daily 500-hPa height anomalies over the Northern Hemisphere onto the loading pattern of the NAO, which is defined as the first leading mode in the rotated empirical orthogonal function analysis. The other index, from the National Oceanic and Atmospheric Administration (NOAA)/Earth System Research Laboratory (ESRL)/Physical Sciences Division (PSD) (https://www.esrl.noaa.gov/psd/data/timeseries/daily/NAO), was constructed by the difference between daily 500-hPa GPH anomalies averaged over two fixed domains (35°N–45°N, 70°W–10°W and 55°N–70°N, 70°W–10°W). Before computing the NAO index, 500-hPa height anomaly fields were reconstructed from the wave components of zonal wave numbers 1–10 in order to emphasize large-scale features. Both NAO indices from July 1, 1957 to June 30, 2014 were used. The modeled NAO index was calculated based on the ESRL/PSD method because of its relative simplicity.

3 | RESULTS

Based on our definition and classification, the numbers of DD- and DS-type events that occurred are 20 and 10 from the NCEP-NCAR reanalysis, 13 and 7 from the MERRA data, and 123 and 55 from the WACCM results, respectively, during the analysis period. These cases were used for a composite analysis in this study. In both the observation datasets and model, DD- and DS-type events accounted for approximately 50% (60% for the model) and 30% of total SSW cases, respectively.

Both DD and DS types are characterized by displacement of the polar vortex off the pole before the central day. After the occurrence of the SSW, however, one waveform persists in the DD type, whereas for the DS type, the polar vortex splits into two small portions (C19). These two DS-type vortexes are usually located over Eurasia and Canada (not shown).

To identify differences in the mean state between the two types, we calculated composite zonal wind difference (Figure 1). We find that the zonal wind in the high-latitude lower stratosphere between 100 hPa and 80 hPa is significantly stronger for DD type than for DS type beginning from a month and a half before the occurrence of the SSW. This stronger wind becomes a weaker polar jet in the upper stratosphere beginning from approximately the central day, although this result was statistically insignificant. There are two significant wind difference maxima from the surface to the lower stratosphere near day −40 and day −10. During these periods, zonal wind for DS type weakens significantly from the surface to lower stratosphere (not shown), which can lead to enhancement of the difference in Figure 1.

To identify any distinctive features in the NAO index between the two types, we plot the temporal evolution of the CPC NAO index smoothed by a 3-day running mean for the two SSW types as shown in Figure 2a. Prior to the central day, the negative NAO phase is predominant for the DS type, whereas the positive NAO phase is dominant for the DD type for prolonged periods. The difference in the evolution of the NAO index between DD and DS types is most pronounced between days −49 and −21. For this period, we further examine the relationship between NAO phase and SSW type (Figure 2b). Based on the CPC NAO index, a positive NAO phase preceded 15 DD-type events out of 20, while a negative NAO phase preceded 9 DS-type events out of 10. However, considering the mean value of the NAO index, the DD-type result is statistically insignificant, whereas the DS-type result is statistically significant. The ESRL/PSD NAO index also

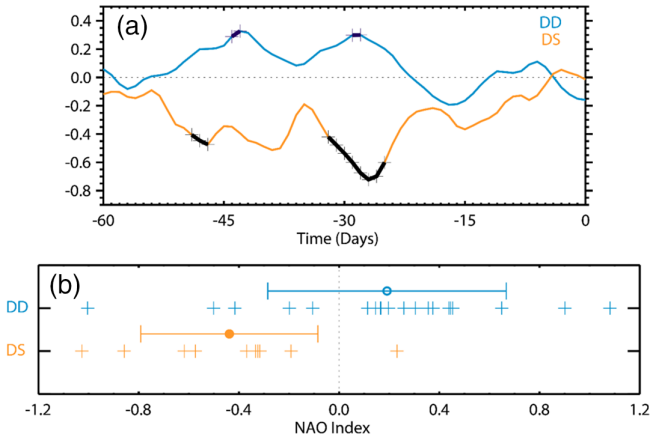

FIGURE 2 (a) Time series of 3-day running-mean NCEP/CPC NAO index. Blue and orange lines denote DD and DS SSW types, respectively. The bold black solid part of each line with crosses indicates statistically significant periods at 95% confidence level. (b) Scatter plot of CPC NAO index occurring during the two SSW types. The NAO index is averaged over days −49 to −21. The mean NAO index for each type is represented by a closed circle with an error bar indicating one standard deviation. A filled circle denotes a statistically significant value at 95% confidence level

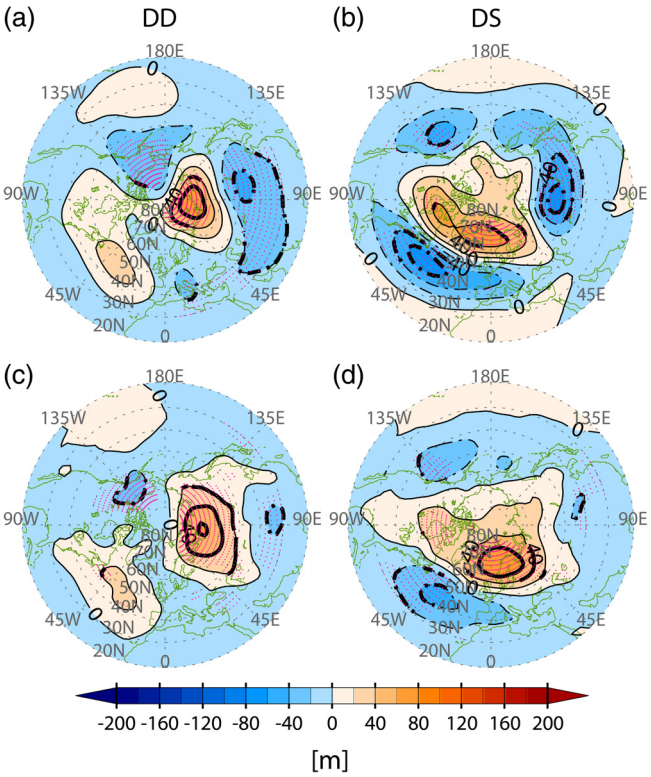

FIGURE 3 NCEP-NCAR GPH anomalies at 500 hPa averaged over days −49 to −21 for (a) DD and (b) DS types. (c) and (d) As in (a) and (b), but for NCEP-NCAR GPH anomalies at 1,000 hPa. The contour interval is 20 m. Bold contours and pink dots indicate statistically significant regions at 95% confidence level

indicates a dominantly negative phase before DS-type SSWs, but the relationship between DD-type SSWs and NAO phase is less clear (not shown). This is because a negative NAO phase can also precede the DD-type SSW events. We also conducted the same analysis, shown in Figure 2, for the SS type. However, the seven SS-type events identified from July 1957 to June 2014 did not have a significant association with a specific NAO phase in the CPC NAO index (not shown).

To examine distinguishable features in the tropospheric pressure pattern between days −49 and −21, we determined the horizontal distributions of the GPH anomaly at 500 hPa (Figure 3a,b). For DD type (Figure 3a), a positive-NAO like pattern occurs in the North Atlantic region, although it is not significant. A prominent positive height anomaly appears across the Ural Mountains and Siberia, and a significant negative height anomaly shows over Chukchi and Bering seas. These patterns seem to be similar to wintertime tropospheric wave-1 height (Garfinkel *et al.*, 2010). For DS type (Figure 3b), on the other hand, the positive height anomaly in the northern part and negative anomaly in the southern part of the North Atlantic resemble the negative NAO pattern, as expected based on Figure 2. The GPH anomaly at 1000 hPa (Figure 3c,d) also shows similar patterns.

Of the 16 SSW events following the positive NAO phase in Figure 2b, 15 events are the DD type. This shows that most DD-type SSW events are preceded by positive NAO phase without the type transition. On the other hand, following the negative NAO phase 5 DD types and 9 DS types of SSW events occur. This reveals that SSW events following the negative NAO phase have a strong tendency to change their type.

To understand the dependence of SSW type-transition on preceding NAO conditions, we examine the temporal evolution of tropospheric GPH wave-1 and wave-2 anomalies and anomalous meridional eddy heat flux representing the vertical component of the Eliassen-Palm flux for DD and DS types following positive (Figure 4) and negative (Figure 5) NAO phases. The NAO phases are determined based on the values averaged over days −49 to −21 in Figure 2b. For extratropical climatological wave-1 height, the ridge (purple contour) is located in the North Atlantic and Eurasia, while the trough (green contour) is identified in Siberia and the North Pacific. For extratropical climatological wave-2 height, the ridges are located over Eurasia and the northeast Pacific, while the troughs are found in the Atlantic and over Siberia, respectively.

Regarding the spatiotemporal evolution of tropospheric wave-1 component following the positive NAO

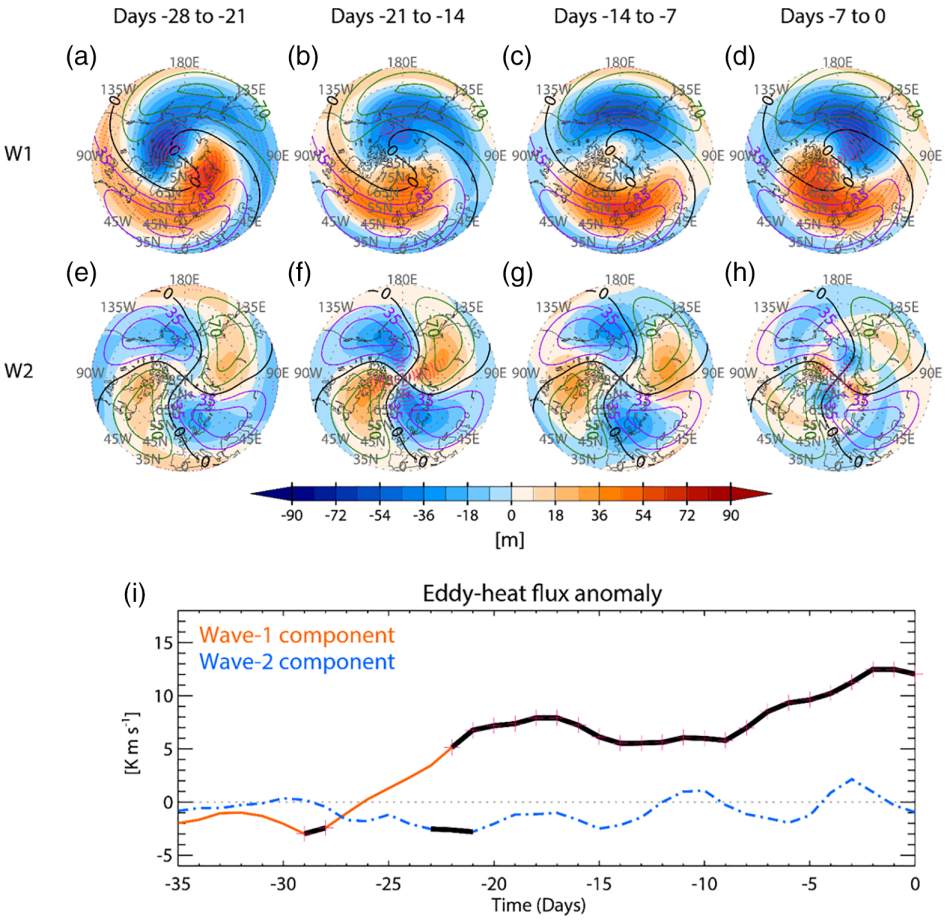

FIGURE 4 (a)–(h) GPH anomalies at 500 hPa averaged over 7 days from days −28 to 0 for DD and DS types following positive NAO phase and climatological DJF-mean value (contour) based on NCEP-NCAR data. (a)–(d) Wave-1 anomaly and (e)–(h) Wave-2 anomaly. The color interval is 9 m and contour interval is 35 m. Purple and green contours denote positive and negative values, respectively. The thick solid contour denotes zero value. Pink dots indicate significantly regions at 95% confidence level. (i) Anomalies of meridional eddy heat flux averaged over 45°N–75°N at 100 hPa for DD and DS types following the positive NAO phase based on NCEP-NCAR data. The orange and blue lines denote contributions by zonal waves 1 and 2 to total eddies. Pink crosses and thick solid part of each line indicate significantly regions at 95% and 90% confidence level, respectively

phase (Figure 4a–d), the ridge over Eurasia and the North Atlantic and the trough over the North Pacific are prominent. This anomalous pattern, in phase with the climatological wave-1 height, can contribute to increase in the magnitude of the climatological wave-1 height. The minor wave-2 anomaly during these periods (Figure 4e–h), however, is out of phase with the climatological wave-2 height and leads to decrease in the amplitude of the climatological wave-2 height. The collocation of the anomalous waves can modulate the vertical wave flux (Garfinkel *et al.*, 2010). Figure 4i shows that the wave-1 component in the heat flux anomaly begins to increase by approximately day −21 before the central day. However, the role of the wave-2 component in the heat flux anomaly is marginal throughout the period.

Regarding the spatiotemporal evolution of tropospheric wave-1 component following the negative NAO phase (Figure 5a–d), the ridge grows around the northern part of the North Atlantic with time and extends across North America and Eastern Europe, while the trough develops across Siberia and the Bering Sea. Although the wave-1 anomaly component produced by the North Atlantic anomaly is confined poleward as compared to the climatological wave-1 height, the similarity between the anomalous and climatological stationary wave patterns might lead to an increase in vertical wave flux as shown in Figure 5i. One noteworthy point is that the wave-2 anomaly (Figure 5e–h) is in phase with the climatological wave-2 height, a few days before the central day. This pattern can help enhance wave-2 height and contribute to increase in the vertical wave flux (Figure 5i), responsible for splitting of stratospheric polar vortex.

We examined the evolution of anomalous meridional eddy heat flux depending on SSW types in our previous work (Figure 8 in C19). Figures 4i and 5i seem to be similar to the evolution of anomalous meridional eddy heat flux for DD type and DS type, respectively. As discussed above, the evolutions of the tropospheric waves vary, depending on the NAO phase before the central day. The negative NAO phase seems to help develop the wave-2 height before the central day. Therefore, the development of the wave-2 component in the heat flux anomaly prior to the DS-type SSW can be explained by the wave-2 component produced by the North Atlantic anomaly.

Rao *et al.* (2019a) showed that a small scale wave in the troposphere appears a few days before the central day, explaining the elongation and split of the weakened polar vortex for the 2019 mixed-type (displacement to split) SSW based on NCEP-NCAR reanalysis. We do not

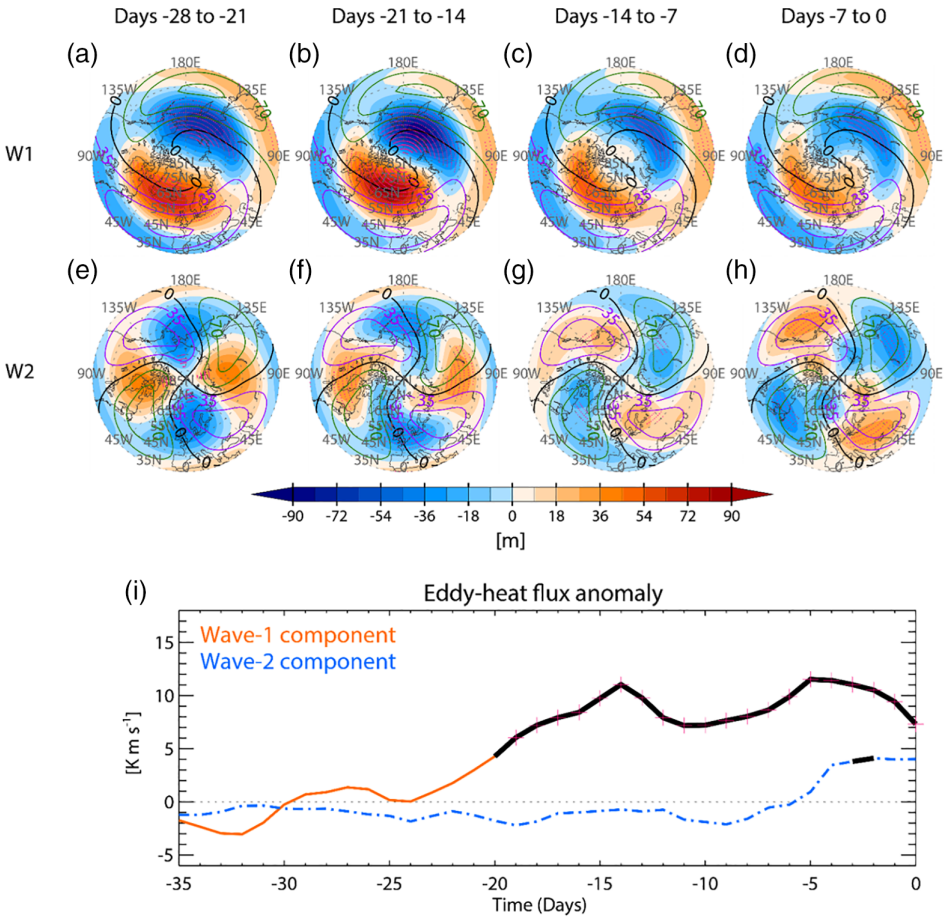

FIGURE 5 As in Figure 4, but for negative NAO

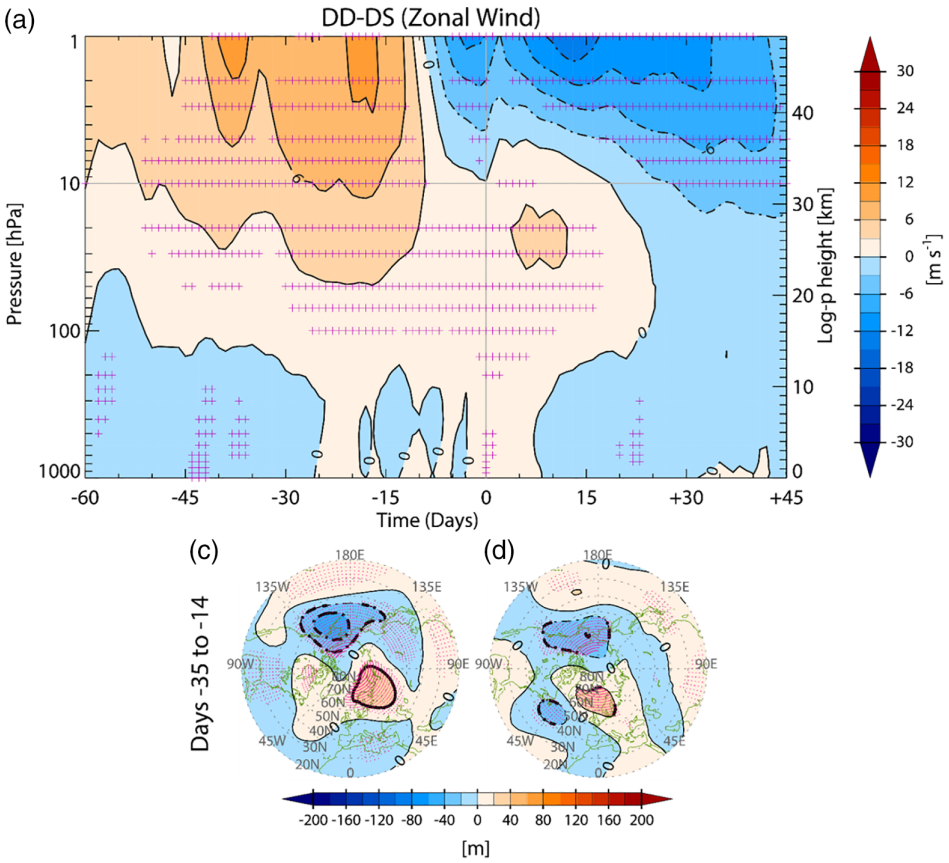

FIGURE 6 (a) As in Figure 1, but for WACCM zonal wind. (b) and (c) As in Figure 3a,b but for WACCM GPH anomalies averaged over days −35 to −14

mean that the preceding NAO phases are the only possible precursors of SSW type transition. This study will enrich existing literature (C19, Rao *et al*., 2019a) by providing the probability that the North Atlantic anomaly can induce a favorable condition for the development of small scale waves and lead to the occurrence of DS-type SSW.

To improve the confidence level of the observational findings described, we perform numerical experiments using the WACCM model. Similar to the observed results described in Figure 1, the modeled stratospheric jet in the lower stratosphere prior to DD-type SSWs is significantly stronger than that of the DS type from approximately days −40 to −15 (Figure 6a). The difference in modeled NAO index between DD type and DS type is relatively large between approximately days −35 and −14 rather than days −49 and −21 (not shown). In other words, the differences in modeled NAO index between the two types are identified as occurring nearer to the central day, while the differences in NAO-related tropospheric patterns are maintained for a shorter period than for the observed results. During this period, approximately two-thirds of all DS-type SSWs correspond to negative NAO phases.

The horizontal distributions of simulated 500-hPa GPH anomalies averaged from days −35 to −14 for each type of SSW as shown in Figure 6b,c. For DD type (Figure 6b), positive anomalies are predominant in the Ural Mountains region and expand to the North Atlantic region, which agrees with the observations. For DS type (Figure 6c), a negative NAO-like pattern occurs in the North Atlantic region, although it is less prominent than in the observed results. Notably, we obtained results similar to the observations using a much greater number of SSW events from the simulation, indicating that our results are robust and compelling.

4 | SUMMARY AND DISCUSSION

In this study, we focus on examining the role of NAO as a precursor for DD- and DS-type SSWs, which account for approximately 80% of total SSW events. The displaced vortex persists for DD type before and after the SSW; however, for DS type, the vortex splits into two after the occurrence of the SSW. We identified significant differences in the strength of the polar stratospheric jet between the two types prior to the SSW event. In the growth stage of SSWs, DS type is characterized by prolonged periods of negative-phase NAO index and tropospheric pressure anomaly fields over the North Atlantic region, which also resembles a negative NAO-like pattern in both reanalysis datasets. The negative NAO phase pattern seems to help develop planetary wave-2 component and consequently leads to splitting of weakening stratospheric vortex. There is a contrasting relationship between DD type and NAO phase to that of DS type. The features of both the DD and DS types observed in the reanalysis dataset were reproduced well by the model, supporting that the observed results are robust.

In conclusion, atmospheric circulation over the North Atlantic region can induce distinct tropospheric-stratospheric dynamical processes for SSWs and act as a precursor to distinguish SSW events, although the mechanism remains uncertain. Understanding the North Atlantic variability would help improve predictability for the occurrence of specific types of SSWs, and also contribute to improved surface weather forecasting.

ACKNOWLEDGEMENTS

This work was funded by a Korea Polar Research Institute (KOPRI) grant under project PE20090 and PE20070. This work was supported by the National Research Foundation of Korea (NRF) grant funded by the Korea government (MEST) (2019R1A2C1005460). WC was supported by the NRF (2018R1A2B6003197).

ORCID

Hyesun Choi https://orcid.org/0000-0002-9298-9148

REFERENCES

Ambaum, M.H.P. and Hoskins, B.J. (2002) The NAO troposphere–stratosphere connection. *Journal of Climate*, 15, 1969–1978. https://doi.org/10.1175/1520-0442(2002)015<1969:TNTSC>2.0.CO;2.

Attard, H.E., Rios-Berrios, R., Guastini, C.T. and Lang, A.L. (2016) Tropospheric and stratospheric precursors to the January 2013 sudden stratospheric warming. *Monthly Weather Review*, 144, 1321–1339. https://doi.org/10.1175/MWR-D-15-0175.1.

Baldwin, M.P., Cheng, X. and Dunkerton, T.J. (1994) Observed correlations between winter-mean tropospheric and stratospheric circulation anomalies. *Geophysical Research Letters*, 21, 1141–1144. https://doi.org/10.1029/94GL01010.

Baldwin, M.P. and Dunkerton, T.J. (1999) Propagation of the Arctic Oscillation from the stratosphere to the troposphere. *Journal of Geophysical Research*, 104, 30937–30946. https://doi.org/10.1029/1999JD900445.

Baldwin, M.P. and Dunkerton, T.J. (2001) Stratospheric harbingers of anomalous weather regimes. *Science*, 294, 581–584. https://doi.org/10.1126/science.1063315.

Charlton, A.J. and Polvani, L.M. (2007) A new look at stratospheric sudden warmings. Part I: climatology and modeling benchmarks. *Journal of Climate*, 20, 449–469. https://doi.org/10.1175/JCLI3996.1.

Choi, H., Kim, B.M. and Choi, W. (2019) Type classification of sudden stratospheric warming based on pre- and postwarming periods. *Journal of Climate*, 32, 2349–2367. https://doi.org/10.1175/JCLI-D-18-0223.1.

Cohen, J. and Jones, J. (2011) Tropospheric precursors and stratospheric warmings. *Journal of Climate*, 24, 6562–6572. https://doi.org/10.1175/2011JCLI4160.1 Corrigendum, 25, 1779–1790. https://doi.org/10.1175/JCLI-D-11-00701.1.

Domeisen, D.I.V., Butler, A.H., Charlton-Perez, A.J., Ayarzagüena, B., Baldwin, M.P., Dunn-Sigouin, E., Furtado, J.C., Garfinkel, C.I., Hitchcock, P., Karpechko, A.Y., Kim, H., Knight, J., Lang, A.L., Lim, E.-P., Marshall, A., Roff, G., Schwartz, C., Simpson, I.R., Son, S.-W. and Taguchi, M. (2019) The role of the stratosphere in subseasonal to seasonal prediction part I: predictability of the stratosphere. *Journal of Geophysical Research: Atmospheres*, 124. https://doi.org/10.1029/2019JD030920.

Garfinkel, C.I., Hartmann, D.L. and Sassi, F. (2010) Tropospheric precursors of anomalous Northern Hemisphere stratospheric polar vortices. *Journal of Climate*, 23(12), 3282–3299. https://doi.org/10.1175/2010JCLI3010.1.

Kalnay, E., Kanamitsu, M., Kistler, R., Collins, W., Deaven, D., Gandin, L., Iredell, M., Saha, S., White, G., Woollen, J., Zhu, Y., Chelliah, M., Ebisuzaki, W., Higgins, W., Janowiak, J., Mo, K. C., Ropelewski, C., Wang, J., Leetmaa, A., Reynolds, R., Jenne, R. and Joseph, D. (1996) The NCEP/NCAR 40-year reanalysis project. *Bulletin of the American Meteorological Society*, 77, 437–471. https://doi.org/10.1175/1520-0477(1996)077<0437:TNYRP>2.0.CO;2.

Karpechko, A.Y., Charlton-Perez, A., Balmaseda, M., Tyrrell, N. and Vitart, F. (2018) Predicting sudden stratospheric warming 2018 and its climate impacts with a multimodel ensemble. *Geophysical Research Letters*, 45(24), 13538–13546. https://doi.org/10.1029/2018GL081091.

Martius, O., Polvani, L.M. and Davies, H.C. (2009) Blocking precursors to stratospheric sudden warming events. *Geophysical Research Letters*, 36, L14806. https://doi.org/10.1029/2009GL038776.

Matsuno, T. (1971) A dynamical model of the stratospheric sudden warming. *Journal of the Atmospheric Sciences*, 28, 1479–1494. https://doi.org/10.1175/1520-0469(1971)028<1479:ADMOTS>2.0.CO;2.

Naujokat, B., Kruger, K., Matthes, K., Hoffman, J., Kunze, M. and Labitzke, K. (2002) The early major warming in December 2001—exceptional? *Geophysical Research Letters*, 29, 2023. http://doi.org/10.1029/2002GL015316.

Neale, R.B., Chen, C.C., Gettelman, A., Lauritzen, P.H., Park, S., Williamson, D.L., Conley, A.J., Garcia, R., Kinnison, D., Lamarque, J.F., Marsh, D., Mills, M., Smith, A.K., Tilmes, S., Vitt, F., Morrison, H., Cameron-Smith, P., Collins, W.D., Iacono, M.J., Easter, R.C., Ghan, S.J., Liu, X., Rasch, P.J. and Taylor, M.A. (2010) *Description of the NCAR Community Atmosphere Model (CAM 5.0). NCAR Technical Note NCAR/TN-486 +STR*. Boulder, Colorado: National Center for Atmospheric Research 282 pp.

Rao, J., Garfinkel, C.I., Chen, H. and White, I.P. (2019a) The 2019 New Year stratospheric sudden warming and its real-time predictions in multiple S2Smodels. *Journal of Geophysical Research*, 124, 11155–11174. https://doi.org/10.1029/2019JD030826.

Rao, J., Ren, R., Chen, H., Liu, X., Yu, Y. and Yang, Y. (2019b) Subseasonal to seasonal hindcasts of stratospheric sudden warming by BCC_CSM1.1(m): a comparison with ECMWF. *Advances in Atmospheric Sciences*, 36, 479–494. https://doi.org/10.1007/s00376-018-8165-8.

Rienecker, M.M., Suarez, M.J., Gelaro, R., Todling, R., Bacmeister, J., Liu, E., Bosilovich, M.G., Schubert, S.D., Takacs, L., Kim, G.K., Bloom, S., Chen, J., Collins, D., Conaty, A., da Silva, A., Gu, W., Joiner, J., Koster, R.D., Lucchesi, R., Molod, A., Owens, T., Pawson, S., Pegion, P., Redder, C.R., Reichle, R., Robertson, F.R., Ruddick, A.G., Sienkiewicz, M. and Woollen, J. (2011) MERRA: NASA's modern-era retrospective analysis for research and applications. *Journal of Climate*, 24, 3624–3648. https://doi.org/10.1175/JCLI-D-11-00015.1.

Taguchi, M. (2018) Comparison of subseasonal-to-seasonal model forecasts for major stratospheric sudden warmings. *Journal of Geophysical Research*, 123, 10231–10247. https://doi.org/10.1029/2018jd028755.

Thompson, D.W.J., Baldwin, M.P. and Wallace, J.M. (2002) Stratospheric connection to Northern Hemisphere wintertime weather: implications for predictions. *Journal of Climate*, 15, 1421–1428. https://doi.org/10.1175/1520-0442(2002)015<1421:SCTNHW>2.0.CO;2.

How to cite this article: Choi H, Choi W, Kim S-J, Kim B-M. Dependence of sudden stratospheric warming type-transition on preceding North Atlantic Oscillation conditions. *Atmos Sci Lett*. 2020;21:e953. https://doi.org/10.1002/asl.953